# A CAD Tool for Optical MEMS

Timothy P. Kurzweg*, Steven P. Levitan*, Philippe J. Marchand**,
Jose A. Martinez*, Kurt R. Prough*, Donald M. Chiarulli***

*University of Pittsburgh, Dept. of Electrical Engineering, Pittsburgh, PA, USA,
tim@ee.pitt.edu, steve@ee.pitt.edu, jmarti@ee.pitt.edu, krpst5@ee.pitt.edu
**University of California, San Diego, ECE Dept., La Jolla, CA, USA, philippe@ece.ucsd.edu
***University of Pittsburgh, Dept. of Computer Science, Pittsburgh, PA, USA, don@cs.pitt.edu

## 1.0 ABSTRACT

**Chatoyant models free-space opto-electronic components and systems and performs simulations and analyses that allow designers to make informed system level trade-offs. Recently, the use of MEM bulk and surface micro-machining technology has enabled the fabrication of micro-optical-mechanical systems. This paper presents our models for diffractive optics and new analysis techniques which extend Chatoyant to support optical MEMS design. We show these features in the simulation of two optical MEM systems.**

## Keywords:

Optical MEMS, MEMS-CAD, MOEMS, micro-optics

## 2.0 INTRODUCTION

Applications for optical MEMS (micro-electrical-mechanical systems) are growing to include scanning, projection, display, switching, printing, sensing, modulating, and data storage.[16] In MEM systems, the role of optics is two-fold. First, MEM actuators can be used to precisely position micro-optical components that perform information processing tasks. Second, optics can be used to evaluate critical alignment and provide feedback on positioning of MEM components.

As these applications are quickly evolving from abstract ideas to marketable products, it is essential to have CAD tools to model these optical MEM systems in order to avoid costly prototyping. In this growing field, technologies are constantly advancing and CAD tools must be flexible in their ability to model and simulate new multi-domain components and systems. Therefore, beyond functional design, a complete optical MEMS CAD tool needs to model electrical and optical signals, mechanical positioning and tolerancing, thermal and vibration effects, fabrication, packaging, and, most importantly, the interaction of all these constraints.

Currently, no single CAD tool completely models the complexity of optical MEM systems. Therefore, designers must use a collection of tools to model, simulate, and analyze each stage of this mixed signal design. For conventional MEM design, a family of CAD tools is emerging, specializing in layout and simulation. Analogy, Inc. has teamed with Microcosm Technologies to create a CAD package to design and simulate MEM systems through Analogy's Saber Tools. Tanner Research, Inc. markets MEMS Pro, which performs layout, error checking, and performance simulation through Tanner's T-Spice. Both of these products use an analog electronic simulation backbone, forcing all system models into electrical templates. Universities have also created specialized tools for MEM modeling and simulation[14][15], and have bridged the gap between CAD and foundry facilities.[5] Recently, new research has addressed the need to synthesize and optimize MEM systems.[10] However, no system level tools have been developed to address the additional constraints imposed by micro-optical systems. This is the focus of our current work.

We have created Chatoyant, a CAD tool that has been successfully used to design and simulate free space opto-electronic interconnect systems.[7][8] Chatoyant is a mixed signal CAD tool, capable of performing end-to-end system simulations while providing the user with a variety of analysis techniques.

In this paper, we first present an overview of Chatoyant and the extensions needed to model optical MEM systems. Next, we introduce our modeling techniques for scalar optics and micro-components that are used as building blocks in optical MEM system design. We then focus on two optical MEM systems simulated with Chatoyant and present results that illustrate our model implementations and analysis techniques.

## 3.0 CHATOYANT

Chatoyant is a mixed-signal opto-electronic simulation framework, built upon the simulation engine, Ptolemy[3]. Chatoyant, can be used to design, simulate, and analyze free space opto-electronic interconnect systems by performing both static and dynamic simulations. Static simulations analyze mechanical tolerancing, power loss, insertion loss, and crosstalk, while dynamic simulations are used to analyze data streams with techniques such as noise analysis and bit error rate (BER) calculation.

In Chatoyant, component models are written in C++ with sets of user defined parameters for the characteristics of the component. Using the synchronous data flow (SDF) and the dynamic data flow (DDF) domains in Ptolemy, we have defined our own message


DAC 99, New Orleans, Louisiana

class to support both optical and electrical signals. This class defines optical signals through their position, direction, intensity, wavelength, and wavefront. Electrical signals are defined by their voltage, output conductance, and output capacitance. The last two parameters are used for impedance matching between electrical signals. These signals are modeled using piece-wise linear discrete event techniques providing user control for accuracy and computation time.[9]

Chatoyant has four component libraries, one for each of the multiple domains supported by our system. The Opto-Electronic Library includes vertical cavity surface emitting lasers (VCSELs), multiple quantum well (MQW) modulators, and p-i-n detectors. The Optical Library, contains components such as lenses, lenslets, mirrors, and apertures. The Electrical Library include CMOS drivers and transimpedance amplifiers, and the Mechanical Library contains actuators, scanning mirrors and other electro-static devices.

In order to support optical MEM design, simulation, and analysis, we have extended Chatoyant in three ways. First, we introduced modeling techniques for diffractive optics. Second, we have included models for micro-lenses, micro-mirrors, phase masks, micro-mechanical actuators, and micro-mechanical mirrors. This allows us to simulate complete optical MEM systems in a single mixed signal framework. An additional requirement emphasized by these microsystems is support for tolerancing on the precise alignment required for desired operation. Therefore, our third extension is the implementation of a Monte Carlo tolerancing package within Chatoyant to determine worst case mechanical tolerancing and sensitivity.

In the next section, we present background on scalar wave theory and develop our models for diffraction analysis. We then move on to show the use of these models in system level simulations.

# 4.0 SCALAR DIFFRACTIVE MODELS

When an optical system's component sizes and propagation distances approach the scale of the wavelength of light, simple geometric and Gaussian propagation approximations are no longer valid. To accurately describe these systems, scalar wave modeling is needed.[4] The scalar equations are directly derived from Maxwell's Equations. These equations can be recast and simplified by assuming that the dielectric medium is linear, isotropic, homogeneous, and nondispersive. This reduction results in all components in the electric and magnetic field summarized as the scalar wave equation:

$$\nabla^2\vec{U} - \frac{n^2\partial^2\vec{U}}{c^2\,\partial t} = 0$$

For monochromatic light, $U(P,t)$ is the positional complex wave function, where $P$ is the position of a point in space:

$$U(P,t) = a(P)e^{j\varphi(P)}e^{j2\pi\nu t}$$

By placing the positional complex wave function into the scalar wave equation, the result is the time-independent Helmholtz equation:

$$(\nabla^2 + k^2)U(P) = 0, \text{ where } k = \frac{2\pi}{\lambda}$$

Two approximations of wave propagation based on diffraction theory are the Fresnel and the Fraunhofer approximations. Both use

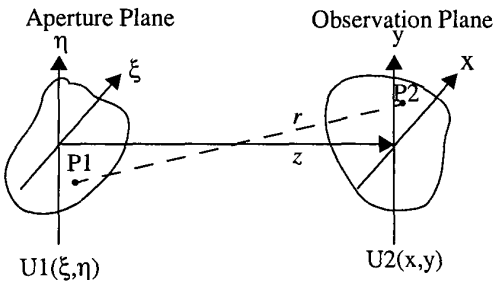


Figure 1: Diffraction Geometry for Fresnel and Fraunhofer Approximations

the Huygens-Fresnel principle, which states that every unobstructed point of a wavefront is a source of spherical wavefronts with the same frequency of the primary wave. The difference between the two approximations is the location of the observation plane, either in the near field (Fresnel approximation) or the far field (Fraunhofer approximation). Using Fresnel diffraction, the curvature of the spherical wavefront is necessary to model. However, with Fraunhofer diffraction, the propagation distance is assumed to be large enough such that the spherical waves have spread into plane waves by the time they strike the observation plane.

Figure 1 shows the geometry of both the Fresnel and Fraunhofer approximations. The distance between the two planes, $z$, determines if the propagation is in near or far field. The object plane is in the near field when $z < 2D^2/\lambda$, where $D$ is the diameter of the aperture, and in the far field otherwise. The figure shows how the spherical wave point source *P1* (from the complex wave function $U1(\xi,\eta)$) in the aperture plane effects *U2(x,y)* at *P2* in the observation plane. All the points in the observation plane determine the new complex wave function, $U2(x,y)$. Both planes are in rectangular coordinates, with the aperture and observation planes defined as $(\xi,\eta)$ and $(x,y)$, respectively. The distance between *P1* and *P2* is $r$.

The Fresnel approximation, shown below, models the spherical waves by the quadratic-phase exponential, the first exponential found in the integral below. To approximate the distance $r$, a binomial expansion of the square root is used, and some of the higher order terms are neglected.[2]

$$U2(x,y) = \frac{e^{jk\left(z+\frac{x^2+y^2}{2z}\right)}}{j\lambda z}\cdot\int_{-\infty}^{\infty}\int U1(\xi,\eta)e^{\frac{jk}{2z}(\xi^2+\eta^2)}e^{\left(-\frac{jk}{z}\right)(x\xi+y\eta)}\,d\xi\,d\eta$$

When the far field approximation is valid, the Fresnel equation greatly simplifies into the Fraunhofer approximation. In this case, the quadratic phase exponential is approximately unity over the entire aperture (a plane wave). The Fraunhofer equation reduces to a Fourier transform of the aperture, therefore, common FFT algorithms are used to solve this approximation. However, for micro-optical systems, we are often required to calculate the wave function in the near field. Therefore, we use the full Fresnel approximation above.

# 5.0 SCALAR COMPONENT MODELS

Using the derivations above, we have modeled light propagating through different diffractive devices, including apertures, lenses, and computer generated holograms. This section describes the models of some of these diffractive elements and compares the propagation of light through a circular aperture and a Fresnel lens.

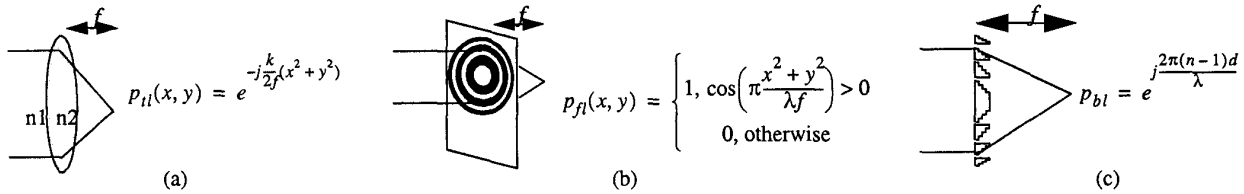


Figure 2: (a) Refractive Lens, (b) Fresnel Lens, (c) Multiple Level Binary Lens

## 5.1 Apertures and Lenses

For modeling apertures, the Fresnel diffraction approximation is solved with the integral limits being defined by the aperture. If there are multiple apertures, the superposition principle applies, and each point in the observation plane is the sum of the outputs obtained when each independent aperture acts alone. For the case of an arbitrary shaped aperture, the aperture is broken into smaller rectangular pieces, and is treated as multiple apertures.

Both refractive and diffractive lenses are used in micro-optical systems. Examples of a refractive and diffractive lenses are given in Figure 2. In each case, the outline of a plane wave striking the lens and converging to the focal point is added to the figure. To model a light wave propagating through a lens, the phase function, $p$, is multiplied by $U1$, the complex wave function, in the propagation integral above.

Refractive lenses act as a phase transformation, resulting when optical beams propagate through different indices of refraction. To model refractive lenses, we confine the lens' phase function with an aperture, usually circular. As seen in Figure 2(a), the phase function of a refractive thin lens, $p_{tl}$, is dependent on the lens' focal length, $f$, and wave number, $k$. We note that even refractive lenses produce diffractive effects when the beam is clipped, as shown later in this paper.

On the other hand, diffractive lenses are designed to change both the light's intensity and phase, causing the light to interfere and form a focused spot. These lenses have advantages over standard refractive lenses in micro-optic systems. Through the fabrication of the diffractive lens, the focal length can be precisely defined within a wide range of numerical apertures, the thickness of the lens can be on the order of an optical wavelength, and the diameter can be on the order of tens of microns.[16]

A Fresnel lens, shown in Figure 2(b), is composed of bands of material that allow or restrict the propagation of the complex light wave. These diffracting rings affect the light wave such that the pattern acts as a spherical lens with an exact focal length. However, the efficiency of these lenses is very low. To simulate the lens, the transmission property of the rings are multiplied by the complex wave function. This transmission property can be thought of as a 0 (opaque band) or 1 (transparent band) phase function, $p_{fl}$, as found in Figure 2(b).[13]

For the multiple level binary lens, shown in Figure 2(c), a phase change occurs based on the thickness of the lens. Since the lens is composed of varying thicknesses, we model this lens as a grid of phase masks, where each grid has a constant thickness. The phase function of each grid, $p_{bl}$, found in Figure 2(c), is determined by the wavelength of the light, $\lambda$, the index of refraction, $n$, and the thickness of the material, $d$. The efficiency of these lenses is greater than the Fresnel lenses, but at a cost of a more complicated fabrication process.

## 5.2 Comparing an Aperture and Fresnel Lens

As an example of diffractive analysis, we propagate a plane wave through both a circular aperture and a Fresnel lens to an observation plane in the near field. Both apertures are 200 μm in diameter, with the Fresnel lens designed to have a focal length of 400 μm, where the observation plane is set.

The radius intensity profile of both the aperture and the Fresnel lens at the observation plane is shown in Figure 3. Notice, that both devices "focus" the plane wave, resulting in a Gaussian shaped main lobe at the observation plane. Airy rings, common to circular apertures, are shown off the main lobe. However, as expected, the Fresnel lens is able to focus the lens to a smaller, tighter beam, without the abundance of extra diffractive lobes. The Fresnel lens' output also has a higher relative peak intensity, however, the circular aperture's output contains more optical power over the 10 μm area of detection. This is not surprising due to the low efficiency of a Fresnel lens, as the opaque bands block part of the propagating light. This example shows how apertures can be used in optical systems as simple "pin-hole" lenses.

# 6.0 OPTICAL MEMS SIMULATION

This section describes two optical MEM systems that have been simulated with Chatoyant. We used the first to illustrate the critical mechanical tolerancing required for optical MEMS, and the second to show how we model a system with micro-mechanical components. These systems highlight the extensions that have been added to Chatoyant for optical MEM simulation and analysis.

## 6.1 High Speed FFT Design

We are part of a team designing, building, and analyzing micro optical systems, with our current project being an optical MEM system performing a high speed FFT, shown in Figure 4. The design is based on integrating a compact interconnect optical system together with two functional logic blocks. The logic blocks perform the necessary computations, and the optics perform a butterfly shuffle. Each logic block is composed of a stack of 16 CMOS processor dice, bonded in a substrate-isolation-substrate sandwich, creating a cube. Bonded to the edge of the processor

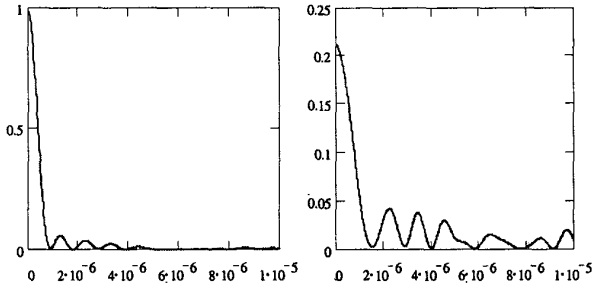


Figure 3: Radius Intensity Profile of (a) Fresnel Lens (b) Circular Aperture

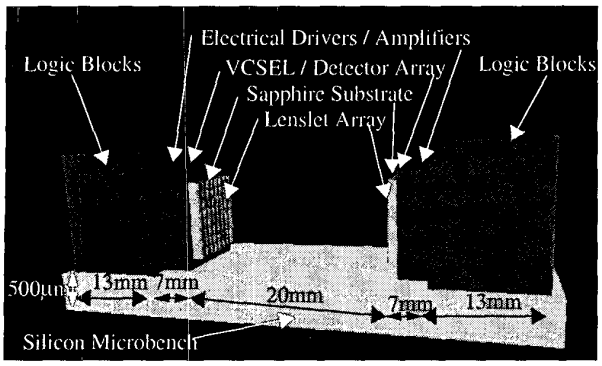


Figure 4: FFT Optical MEM System

stack, is the VCSEL/Detector opto-electronic sub-system. Since the system is bi-directional, each stack has extra circuitry to drive the VCSELs and amplify the received data from the photodetectors. The sources and detectors are placed in an array that allows parallel data transmission. The components are placed onto a substrate, and are held and aligned using conventional MEM technology. Figure 4 is a screen shot of the FFT system created by a VRML (Virtual Reality Modeling Language) interface that we are incorporating into Chatoyant.

### *6.1.1 VCSEL Mechanical Tolerancing*

We simulate a single VCSEL-to-detector interconnect to determine the mechanical tolerancing of the VCSEL position during fabrication. This simulation illustrates the sensitivity of micro-optic systems to minor offsets in components' positioning. Scalar diffractive models have to be used since there are no simple Gaussian approximation models for off-axis clipping.

To simulate positional tolerancing, the VCSEL sources are offset by 1 μm in the $x$ direction, causing off-axis clipping between the beam and the first lenslet. With such a small offset, the clipping at the first lenslet array is almost identical to the case for no offset (a power loss of 4.53%). As the light propagates 20mm to the second lenslet, the positional displacement of the 1 μm offset beam grows to approximately 40μm, as seen in Figure 5. The figure shows the intensity contour of the beam at the second lenslet with the approximate size (250 μm) and position of the lenslet superimposed on the contour graph. Much of the beam passes through the second lenslet, although, 22.6% of the remaining power is lost, resulting in a total system insertion loss of 26.1%. Figure 6 shows the $x$-axis intensity distribution at the 80 μm detector. The shape of the beam

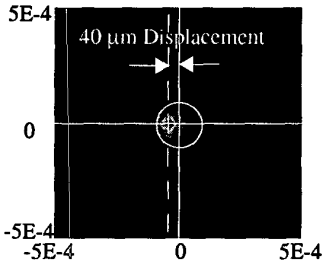


Figure 5: Intensity distributions of a 1μm VCSEL Offset Propagated 20mm to the Second Lenslet Array

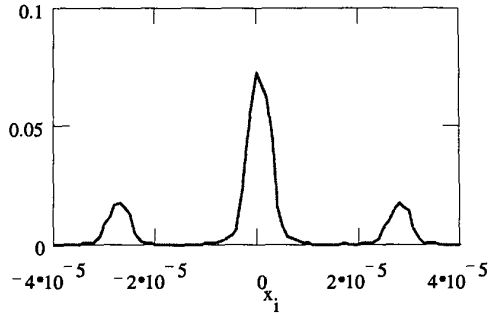


Figure 6: Scalar Intensity Distribution at the 80 μm Detector

is no longer Gaussian, as visible side lobes are present. Note that the lens has steered the beam back onto the detector, with the center of the beam shifted off-axis only 1 μm. Also, note that the side lobes are almost at the full radius of the detector, therefore, for some cases, these lobes will miss the detector, resulting in an even greater insertion loss. If the initial VCSEL beam is offset by 5 μm, the offset grows to almost 200 μm at the second lenslet. With such a large axial offset, the beam misses the second lenslet, and the signal never reaches the detector. This illustrates the need for critical alignment tolerances in these micro-optical systems.

In general, it is hard to predict for what cases or offsets will give the worst case behavior in a complex system. Therefore, a standard technique is to use Monte Carlo analysis simulations [12] that vary the mechanical properties (position and orientation) of each of the components according to a probability distribution based on manufacturing tolerances, mechanical vibration, and thermal expansion. In the next section, we discuss extensions to Chatoyant to support mechanical tolerancing analysis.

### *6.1.2 Monte Carlo Analysis*

Chatoyant allows the designer to use probability distributions (e.g., linear, Gaussian, or Poisson) instead of specific values for component parameters. During Monte Carlo simulation, Chatoyant runs the system multiple times using the specified distribution for component parameter values, analyzes the outputs in terms of output power detected, and returns sets of system parameters that lead to sensitivity analysis of component parameters.

A 3x3 sub-system of Figure 4 is simulated using Chatoyant's Monte Carlo analysis. In this simulation, the VCSEL positions are held constant as a reference geometry for the system, and the parameters for the other components are given in the first row of Table 1. As seen, there are ten tolerancing parameters in the system, making sensitivity analysis of the individual parameters to the system performance difficult. Each of the ten parameters are varied with a Gaussian distribution, specified by a mean of zero and a variance found in the table. After running the Monte Carlo analysis for 10,000 simulations, we analyze which cases have the largest deviation in parameters, but detect full optical power, and the cases where the parameters deviate the least, but result in the beam entirely missing the desired detector. The 10,000 random simulations with ten degrees of freedom completed in about 80 minutes, running on a 300 MHz machine running Linux. We examine the runs in which full power is detected (1,653 out of 10,000 runs), sort them by maximum parameter deviation, and report the top two cases in Table 1 (Full Power #1 and #2). Similarly, we examine

**Table 1: Monte Carlo Analysis Results**

| Parameter | Lens1_x (μm) | Lens1_y (μm) | Lens1_ρ (°) | Lens1_θ (°) | Lens2_x (μm) | Lens2_y (μm) | Lens2_ρ (°) | Lens2_θ (°) | Detect_x (μm) | Detect_y (μm) |
|---|---|---|---|---|---|---|---|---|---|---|
| Variance | 1μm | 1μm | .05 | .05 | 1μm | 1μm | .05 | .05 | 1μm | 1μm |
| Full Power #1 | -0.6070 | -0.5874 | -0.05609 | -0.02963 | 0.5546 | 0.6080 | -0.03642 | 0.02904 | -0.4623 | -0.9546 |
| Full Power #2 | 0.4638 | -0.3931 | 0.01526 | -0.00759 | 0.4182 | 0.4242 | -0.01232 | -0.01138 | -0.3922 | 0.6849 |
| No Power #1 | 0.3951 | 1.1671 | -0.00452 | **0.00765** | -0.4086 | -0.2473 | 0.00394 | -0.00029 | -0.6104 | -0.8974 |
| No Power #2 | -0.4966 | 1.5536 | -0.00895 | 0.00401 | 0.9910 | 0.3492 | 0.00975 | **-0.01081** | 0.2230 | 0.4476 |

the runs in which at least one beam completely missed its desired detector (6,921 out of 10,000 runs), sort these in terms of minimum parameter deviation, and report the top two (No Power #1 and #2). When the beam completely misses the detector, we conclude the most common cause is the tilts (ρ or θ) of the lenses. This is shown in Table 1 by the largest normalized parameter in each run, typed in bold, being a lens tilt. Notice, for most parameters, the offsets of the runs Full Power #1 and #2 are larger than the parameter offsets for No Power #1 and #2. This is due to the system parameters compensating for each other. That is, if one parameter steers the beam out of the optical path, another parameter compensates by steering the beam back in line.

## 6.2 Scanning Mirror Optical MEM Systems

Another optical MEM system using the same processor stacks and opto-electronic devices, found in Figure 4, is shown in Figure 7. Here as shown with dashed lines, the light is propagating vertically through a prism and reflecting off a plane mirror. The light is then reflected off of an optical MEM scanning mirror, back to the plane mirror, and captured on detectors. In this system, the scanning mirror can be used both for alignment and switching.

The scanning mirror is a micromachined 2D mirror built upon a Micro Elevator by Self Assembly (MESA) structure.[11] The mirror and MESA structure are shown in Figure 8(a) and (b), respectively. The scanning mirror can tilt in both the *x* and *y* directions, along the torsion bars, and is controlled electrostatically through four electrodes beneath the mirror, outlined in Figure 8(a) by the dashed boxes. For example, the mirror tilts in the positive *x* direction when voltage is applied to electrodes 1 and 2, and the mirror tilts in the negative *y* direction when voltage is applied to electrodes 1 and 4. The MESA structure is shown in Figure 8(b). The mirror is elevated by four scratch drive actuator (SDA)[1] arrays pushing the support plates together, allowing for the scanning mirror to buckle and rise up off the substrate. The MESA structure's height is required to be large enough such that the tilt of the mirror will not cause the mirror to hit the substrate. System alignment can also be possibly aided by this MESA structure.

With the flexibility of the scanning mirror, this system could act as a switch, an optical scanner, or a reconfigurable optical interconnect. Using a sub-system of the design shown in Figure 7, we have simulated systems using this scanning mirror configuration for switching and self-alignment through optical feedback.[6] Here, we demonstrate an optical scanning system.

For this scanning system, we use a single source beam propagating through a 3x3 sub-system of Figure 7. With the appropriate voltage levels applied to the four electrodes, the scanning mirror tilts and directs the single source to any of the nine detectors. This system, as represented in Chatoyant, is shown in Figure 9. Each icon represents a component model with sets of parameters defining the characteristics of the component and each "wire" represents a signal path (either optical or electrical) connecting the outputs of one component to the inputs of the next. The SDA arrays move the mirror to the correct height for alignment. We control the electrodes with a waveform generator, which applies the appropriate voltages on the four electrodes for the beam to scan or switch in a desired pattern. As an example, we are able to scan a diamond pattern with the waveforms shown in Figure 10. The desired pattern is shown by the white arrow trace on the first output image. The other 9 images show snapshots of the detector plane as the diamond pattern is scanned. Dashed lines with letters correspond time intervals in the waveforms and in the snapshots. Mechanical alignment is again critical in this system. For example, the lenslets in this simulation are only 100 μm in diameter. Therefore, when steering the beam, precision in the voltage waveforms is needed so that the light, bending through the prism, hits the desired detector's lenslet.

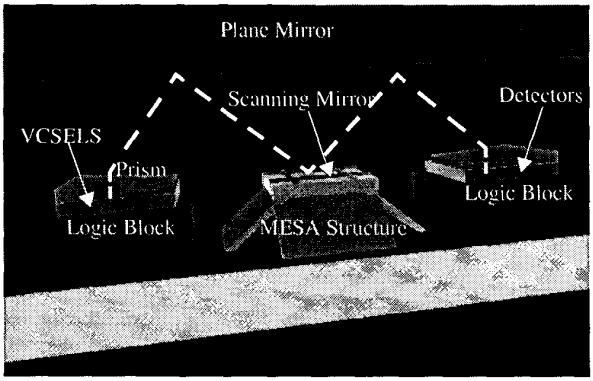


Figure 7: Other system using optical MEM scanning mirror

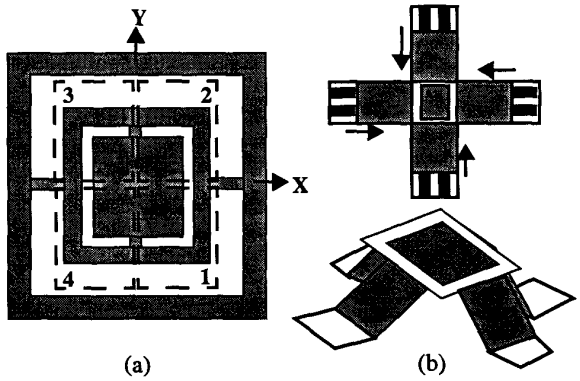


Figure 8: (a) Scanning Mirror and (b) MESA Structure[11]

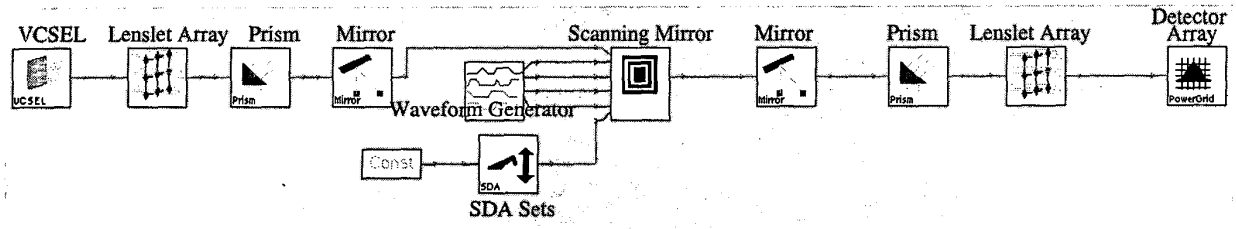


Figure 9: Scanning Mirror System in Chatoyant

## 7.0 SUMMARY AND CONCLUSIONS

The multiple technologies (optical, electrical, and mechanical) utilized in optical MEM systems, make it difficult to create a complete optical MEMS CAD tool. This paper has shown the extensions, in particular the diffractive models, new micro-optical and mechanical components, and mechanical tolerancing using Monte Carlo analysis, that have been added to Chatoyant to enable the modeling of micro-optical systems.

Chatoyant's ability to perform and analyze optical, electrical, and mechanical trade-offs make our system valuable to optical MEM designers. Keeping all the simulations internal to the Chatoyant framework allows for quick and efficient analysis throughout multiple domains. Results from system simulations show that Chatoyant is a useful, practical alternative to costly prototyping optical MEM systems.

We would like to acknowledge the support of DARPA contract number F3602-97-2-0122 and NSF grant ECS-9616879.

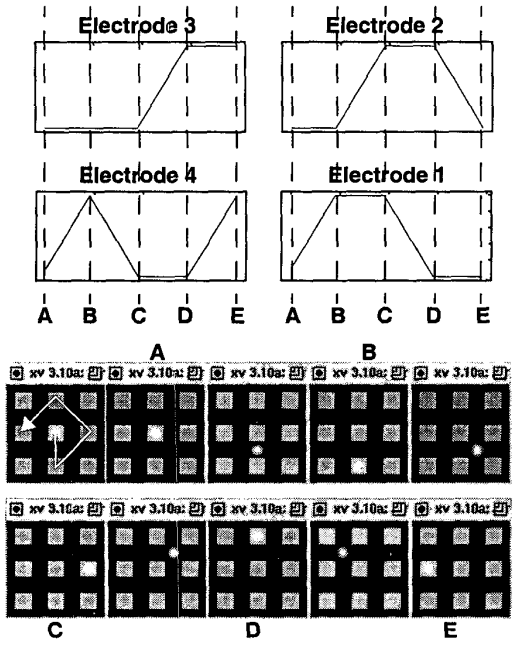


Figure 10: Waveforms and Snapshots of Scanning Pattern

## 8.0 REFERENCES

[1] Akiyama, T., et. al, "Scratch drive actuator with mechanical links for self-assembly of three-dimensional MEMS," *J. of Microelectromechanical Systems*, Vol. 6, No. 1., Mar 1997, pp. 10-17.

[2] Born, M., Wolf, E., Principles of Optics, (Pergamon Press, 1959)

[3] Buck, J., et.al, "Ptolemy: a framework for simulating and prototyping heterogeneous systems," *Int. J. Computer Simulation*, Vol. 4, pp. 155-182, (1994).

[4] Goodman, J.W., Introduction to Fourier Optics, Second Edition (The McGraw-Hill Companies, Inc., 1996).

[5] Karam, J.M., et. al, "CAD and foundries for microsystems", 34th DAC, Anaheim, CA, June 9-13, 1997, pp. 674-679.

[6] Kurzweg,T.P., et. al "Modeling Optical MEMS Systems,", TR99-103, University of Pittsburgh, 1999.

[7] Levitan, S.P., et al, "Chatoyant: a computer-aided design tool for free-space optoelectronic systems," *Applied Optics*, Vol. 37, No. 26, Sept 1998, pp. 6078-6092.

[8] Levitan, S.P., et. al, "Computer-Aided Design of Free-Space Opto-Electronic Systems," 34th DAC, Anaheim, CA, June 9-13, 1997, pp. 768-773.

[9] Martinez, J.A., et. al, "Piecewise Linear Large Scale Models for Optoelectronic Devices," OSA Optics in Computing, Aspen, CO, Apr 1999.

[10] Mukherjee, T., Fedder, G.K., "Structured Design Of Microelectromechanical Systems," 34th DAC, Anaheim, CA, June 1997, pp. 680-685.

[11] Piyawattanametha, W., et. al, "MEMS Technology for Optical Crosslink for Micro/Nano Satellites," NANOSPACE'98, NASA/Johnson Space Center, Houston, TX, Nov 1-6, 1998.

[12] Rubinstein, R.Y., *Simulation and the Monte Carlo Method*, (John Wiley & Sons, 1981).

[13] Saleh, B.E.A., Teich, M.C., Fundamentals of Photonics (New York: Wiley-Interscience, 1991).

[14] Senturia, S. D., "CAD for Microelectromechanical Systems," Transducers '95, June 25-29, 1995, Stockholm, Sweden, Vol. 2, Paper No. 232-A7.

[15] Wilson, N.M., et. al, "A Heterogenous Environment for Computational Prototyping and Simulation Based Design of MEMS Devices", SISPAD 98, Leuven, Belgium, Sept 2-4, 1998.

[16] Wu, M.C., "Micromachining for optical and Optoelectronic Systems," *Proc. of the IEEE*, Vol. 85, No. 11, Nov 1997, pp. 1833-1856.